Discriminating lava flows of different age within Nyamuragira's volcanic field using spectral mixture analysis

Long LI [1,5*], Frank CANTERS [2], Carmen SOLANA [3], Weiwei MA [4], Longqian CHEN [5], Matthieu KERVYN [1]

1. Department of Geography & Earth System Science, Vrije Universiteit Brussel, Pleinlaan 2, 1050 Brussels, Belgium

2. Cartography and GIS Research Group, Department of Geography, Vrije Universiteit Brussel, Pleinlaan 2, 1050 Brussels, Belgium

3. School of Earth and Environmental Sciences, University of Portsmouth, Burnaby Building, Burnaby Road, Portsmouth, PO1 3QL, UK

4. Shanghai Institute of Technical Physics, Chinese Academy of Sciences, Yutian Road 500, 200083 Shanghai, China

5. School of Environmental Science and Spatial Informatics, China University of Mining and Technology, Daxue Road 1, 221116 Xuzhou, China

*: long.li@vub.ac.be

Abstract

In this study, linear spectral mixture analysis (LSMA) is used to characterize the spectral heterogeneity of lava flows from Nyamuragira volcano, Democratic Republic of Congo, where vegetation and lava are the two main land covers. In order to estimate fractions of vegetation and lava through satellite remote sensing, we made use of 30 m resolution Landsat Enhanced Thematic Mapper Plus (ETM+) and Advanced Land Imager (ALI) imagery. 2 m Pleiades data was used for validation. From the results, we conclude that (1) LSMA is capable of characterizing volcanic fields and discriminating between different types of lava surfaces; (2) three lava endmembers can be identified as lava of old, intermediate and young age, corresponding to different stages in lichen growth and chemical weathering; (3) a strong relationship is observed between vegetation fraction and lava age, where vegetation at Nyamuragira starts to significantly colonize lava flows ~15 years after eruption and occupies over 50% of the lava surfaces ~40 years after eruption. Our study demonstrates the capability of spectral unmixing to characterize lava surfaces and vegetation colonization with time, which is particularly useful for poorly known volcanoes or those not accessible for physical or political reasons.

Keywords: Vegetation fraction; lava flow; spectral mixture analysis; Nyamuragira; ALI; Pleiades

1. Introduction

Volcanic activity poses a persistent hazard to human activities and to the environment. At dominantly effusive volcanoes, frequently occurring lava flows destroy vegetation, cover fertile soils and pose a threat to human lives and properties. Freshly emplaced lava is inhospitable to plant growth (Deligne et al., 2013) and animal activities andthe time of post-eruption vegetation recovery ranges from several years to decades to centuries, even influencing when affected residents return to their previous lands (De Rose et al., 2011). Characterising the timeframe for soil formation and vegetation colonisation of lava flows is hence vital for the estimation of long-term impacts of volcanic resurfacing on agriculture and natural ecosystems. It also provides a framework for volcanic hazard assessment through the evaluation of return periods of volcanic activity.

.

Although the vegetation cover of an area can be studied on the field (Sohn and McCoy, 1997), the synoptic view provided by remote sensing offers great potential for documenting and quantifying the overall dynamic process of vegetation recovery. Remote sensing is also increasingly contributing to monitoring volcanic activities and mapping volcanic terrains, notably for inaccessible volcanoes (Ernst et al., 2008; references therein). Most commonly used satellite images, however, have a relatively coarse spatial resolution, ranging from low (MODIS, 250 m to 1 km) to moderate (Landsat TM/ETM+, 30 m). Pixels at these resolutions are frequently mixed and thus pixel-based classification methods fail to accurately discriminate lava and vegetation. This is especially problematic for lava surfaces, which are characterized by

variable roughness at centimeter to hundred meters scales (e.g. pahoehoe vs aa textures or lava channels and levees). This roughness creates high spatial variability in illumination, temperature, wind and humidity, as well as sediment trapping, which controls mechanically and chemically the weathering of lava flows and the initiation of biological processes. Discriminating spectrally contrasting lava surfaces at sub-pixel resolution and quantifying the spatially heterogeneous vegetation recovery is therefore of great interest and cannot be addressed by traditional classification techniques.

Spectral mixture analysis (SMA) refers to a group of techniques used for extracting the fraction of spectrally pure materials present within mixed pixels. Many SMA related studies focus on mapping vegetation and impervious surfaces in urban areas (Deng and Wu, 2013; Van de Voorde et al., 2009; and referrences therein). The technique has also been applied to non-urban areas (Sohn and McCoy, 1997; Sonnentag et al., 2007; Zhang et al., 2005), but volcanic regions have received scant attention. Existing studies identified endmembers on volcanic deposits (e.g.Ramsey and Fink ,1999) or Heinz and Chang, 2001).but up to now, LSMA has not yet been utilized to investigate the spectral evolution and vegetation colonization of lava surfaces with time. However, the large spectral contrast between the dark lava surfaces and the scattered vegetation growing on them, and potentially between fresh and highly weathered volcanic surfacesmake them an ideal target for applying SMA.

Therefore, in this study we test the potential of LSMA for lava surface discrimination in Nyamuragira's volcanic field. Specific objectives are: 1) to investigate the applicability of LSMA for characterizing lava flows; 2) to identify and interpret contrasted spectral endmembers; and

3) to document the spectral evolution and vegetation recovery patterns on lava flows through time.

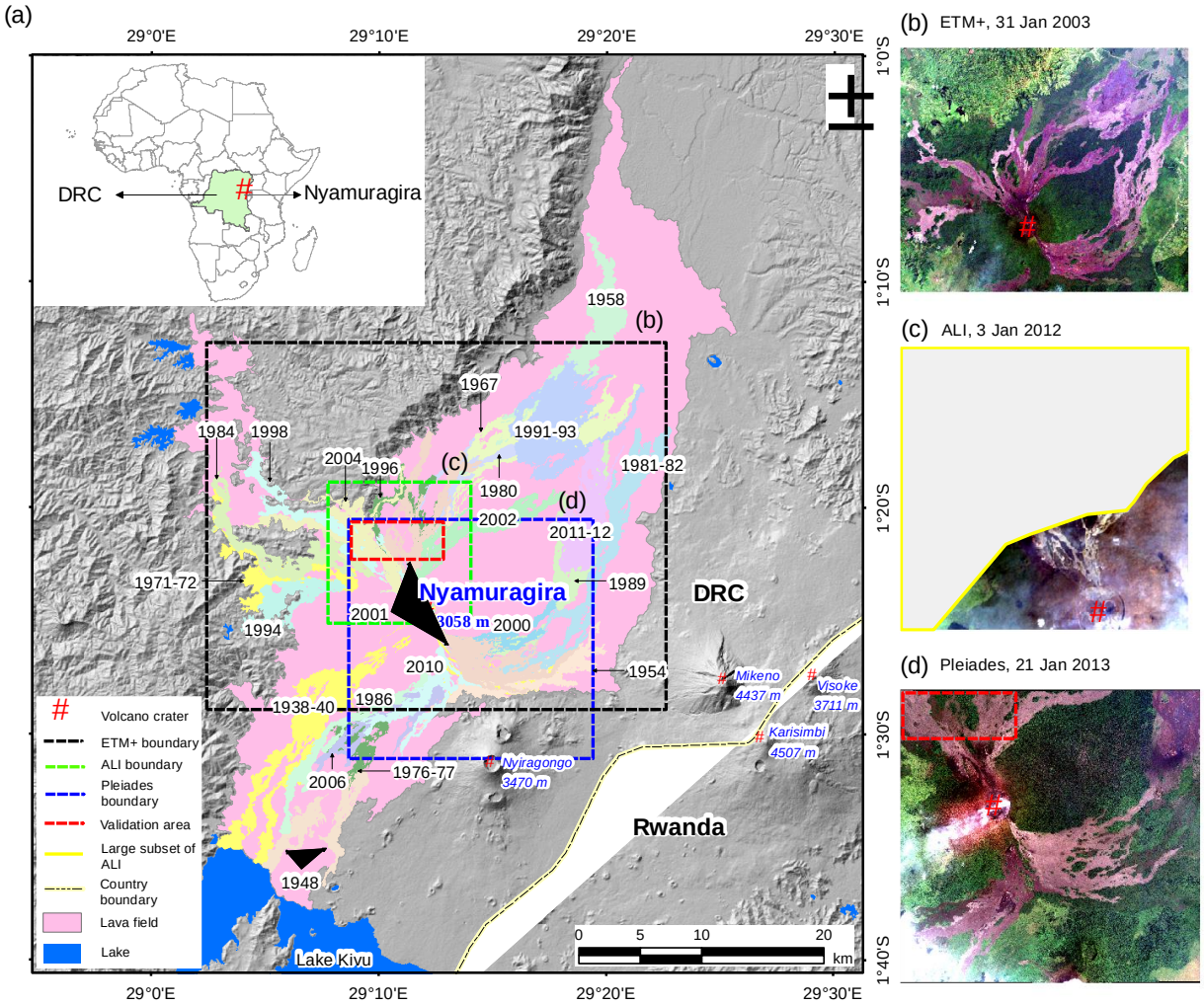

Figure 1 Location map of Nyamuragira volcano showing lava flows erupted between 1938 and 2011 (adapted from Smets et al., (2010)). The three used satellite scenes are displayed in true colors on the right side with their acquisition date. Yellow lines in (c) indicate the extent of the large-scale ALI subset used for spectral unmixing. Red lines in (c) and (d) show the overlap between the ALI and Pleiades images, used for validation of the spectral unmixing results.

2. Study Area

Nyamuragira (Nyamulagira) is an active shield volcano located in the Virunga Volcanic Province of the Democratic Republic of Congo (DRC) (*Figure 1*). It has a maximum elevation of 3058 m a.s.l. and a large lava field that covers over 1100 km^2 (Smets et al., 2010). It is the most active African volcano, presentingeruptions every 2-4 years, an they are well documented with 27 dated and mapped lava flows since 1938 (Smets et al., 2014, 2010).

The composition of Nyamuragira's lavas is very homogeneous over time (removing varietions in composition as a potential endmember) and typical of lavas from the East Africa Rift System (Smets et al., 2014). Due to its equatorial climate, vegetation grows rapidly on Nyamuragira's lavas (*Figure 2*). These characteristics and the limited elevation gradient of the volcano make Nyamuragira an ideal area for studying spectral evolution of lava from the perspective of vegetation recovery.

Political unrest in DRC has hampered ground-based fieldwork since 1994 and remote sensing data have therefore become the main source of information to document the evolution of new volcanic surfaces (Head et al., 2013; Smets et al., 2010).

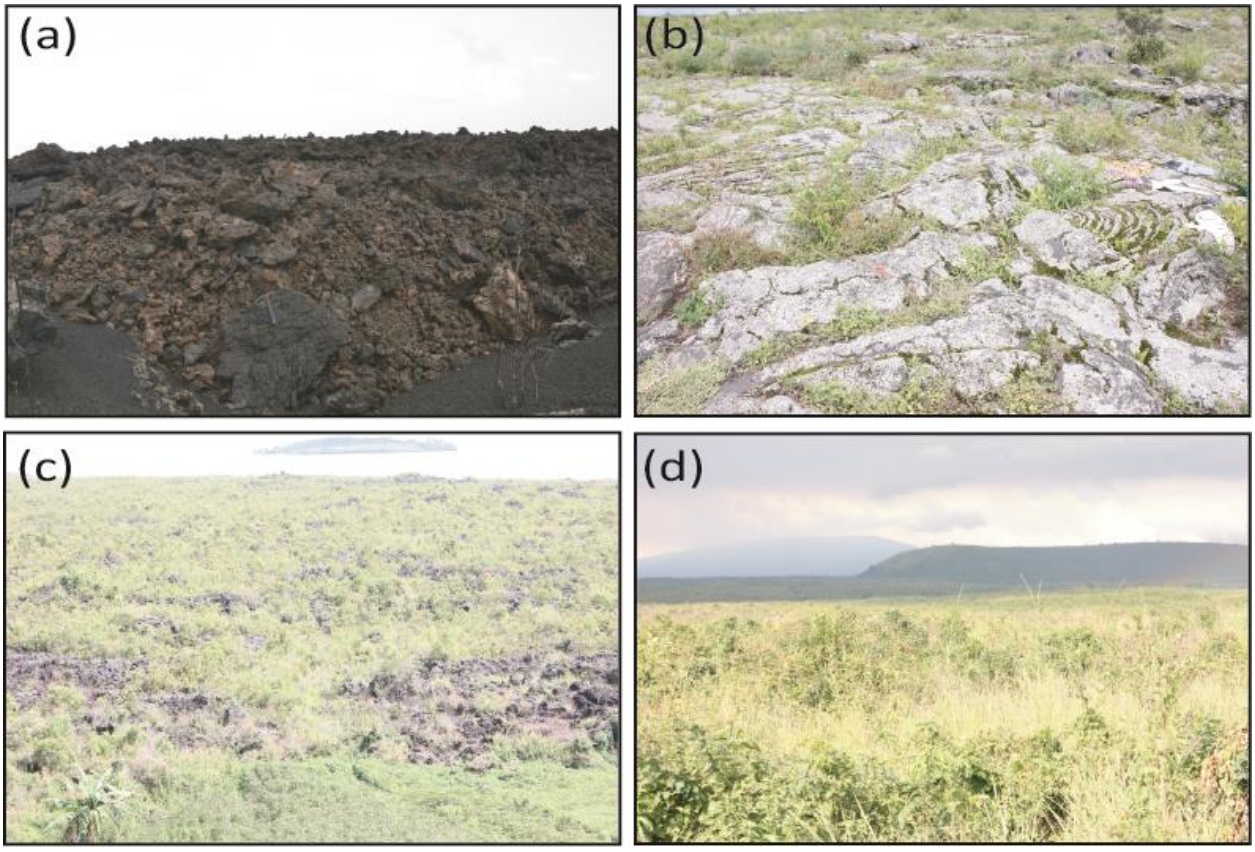

Figure 2 Illustration of the variability of lava surfaces in Nyamuragira's volcanic field: (a) fresh surface; (b) vegetated surface with grey lichens; (c) more strongly vegetated surface; and (d) highly vegetated surface. Photos by Benoît Smets in March 2012 (a) and Sam Poppe in November 2013 (b- d).

3. Data and Methods

3.1 Satellite data

Satellite images used in this study consist of a Landsat Enhanced Thematic Mapper (ETM+) image acquired on January 31, 2003, an Advanced Land Imager (ALI) from January 3, 2012, and a Pleiades image from January 21, 2013 (*Figure 1*). The ALI and ETM+ images were used for spectral unmixing, while the Pleiades image provided validation. The ALI sensor is characterized by 9 multispectral bands, 6 of which mimic the TM/ETM+ bands. *Table 1* provides detailed

information on the spectral bands and their spatial resolutions (ASTRIUM, 2012; Hearn et al., 2001).

Table 1 Spectral bands and spatial resolutions of EO-1 ALI and Pleiades imagery. The three additional bands of ALI respective to Landsat ETM+ are identified with a "p" in their name.

ALI			Pleiades		
Band	Wavelength(μm)	Resolution(m)	Band	Wavelength(μm)	Resolution(m)
pan	0.480-0.690	10	panchromatic	0.470-0.830	0.5
b1p Violet	0.433-0.453	30	b0 Blue	0.430-0.550	2
b1 Blue	0.450-0.515	30	b1 Green	0.500-0.620	2
b2 Green	0.525-0.605	30	b2 Red	0.590-0.710	2
b3 Red	0.630-0.690	30	b3 NIR	0.740-0.940	2
b4 NIR*	0.775-0.805	30			
b4p NIR	0.845-0.890	30			
b5p NIR	1.200-1.300	30			
b5 SWIR1*	1.550-1.750	30			
b7 SWIR2	2.080-2.350	30			

* NIR: near infrared; SWIR: shortwave infrared.

As a consequence of the equatorial setting and the topographic barrier created by the volcanic edifice, satellite images of Nyamuragira are typically cloud-contaminated. The ETM+ image used in this study was selected as the one with the least cloud cover available over the study area (*Figure 1(b)*). The ALI image was recorded during the November 2011 - March 2012 eruption. As a consequence, part of the forested flanks of Nyamuragira were covered by volcanic tephra, showing brownish colours in the satellite image. However, the image was

selected as it was the only scene with limited cloud cover available within a short time interval (i.e. 1 year) from the acquisition of the high-resolution Pleiades image used for validation. In our analysis, the area affected by tephra fall and gas emission from the eruption was masked out (*Figure1(c)*).

Both moderate-resolution images were processed for spectral unmixing. Only the ALI unmixing results could be validated due to the absence of high-resolution reference data for the period of the ETM+ image acquisition. All the spatial data were co-registered to the Universal Transverse Mercator (UTM) projection with WGS84 datum and UTM Zone 35S. The Pleiades image was orthorectified and the ALI image was co-registered to it with an error less than 10 m. MODTRAN-based radiometric correction was performed with the software package ENVI®4.8 on all the satellite images to minimize atmospheric effects and to obtain more reliable reflectance data.

3.2 Linear spectral mixture analysis (LSMA)

In SMA, the spectrum of a pixel is considered a linear combination of spectra of pure endmembers within the pixel weighted by their fractional abundance. The fraction of each endmember within a pixel is derived by applying a least squares technique to minimize the unmodeled residual error (Van de Voorde et al., 2009; Wu and Murray, 2003). Here we applied a fully constrained LSMA approach, which imposes additional sum-to-unity and non-negativity fraction constrains simultaneously. According to Weng et al. (2004) this produces more accurate endmember fractions. The model fitness can be described by the RMS over all bands (Wu and Murray, 2003).

142 Potential endmembers are obtained from the image feature space that is explored by applying
143 a minimum noise fraction (MNF) transform (Wu and Murray, 2003). In order to minimize intra-
144 endmember spectral variability, Wu (2004) proposes brightness normalization before MNF. This
145 method increases the accuracy of the unmixing (Demarchi et al., 2012; Van de Voorde et al.,
146 2009), and was used in this study to facilitate the definition of endmembers.

147 ***3.3 Accuracy assessment***

148 To quantify the unmixing accuracy, detailed ground reference data are needed (Somers et al.,
149 2011). High spatial resolution image data can be a good alternative for ground truth if
150 exhaustive fieldwork is impossible. In this study, a 2 m Pleiades image was used and classified
151 into a binary map with pixels being labelled as vegetation or lava. Validation samples were then
152 randomly generated in the ALI image. In order to minimize geo-registration errors, the sample
153 unit size in the Ali image was set at 3×3 pixels (following Wu and Murray, 2003), spatially
154 corresponding to 45×45 Pleiades pixels. For each sample unit, the vegetation fraction derived
155 from the ALI image and the vegetation coverage estimated from the Pleiades image was
156 compared. We used mean error (ME) and root mean squared error (RMSE) to evaluate the
157 accuracy of the spectral unmixing for the vegetation fraction estimation (Wu and Murray, 2003).

158 As the available ALI and Pleiades images have a limited overlap (~7.5×3 km^2), validation was
159 exclusively performed on their common area. In absence of image reference data, the unmixing
160 accuracy was not independently assessed for the large-scale subsets of ALI and ETM+, yet both
161 subsets were compared to each other to verify the consistency of the unmixing results for the
162 two scenes, acquired 9 years apart.

4. Results

4.1 Identification of spectral endmembers

Most of the spectral variability in the normalized reflectance data obtained can be explained by the first three MNF components (93.77% for the ETM+ and 81.87% for the ALI). For both datasets, the first two components (MNF1 against MNF2) form a V-shaped distribution with three conspicuous vertices (*Figure 3*). When examining feature subspaces of MNF1 against MNF3 and MNF2 against MNF3 the distributions observed for both datasets present some differences in shape. Vegetation could be easily identified as an endmember in both images. In case of the ETM+ image, pixels located at vertices v1, v4 and v8 mostly correspond to the 1991-93 flow while those at v3 and v7 correspond to the 1981-82, 1984 and 1986, and those at v6 and v9 to the 1998, 2000 and 2001 (*Figure 3*). Hence, these extreme pixels seem to represent lava surfaces of different age. A similar pattern is observed for the ALI image. These pixels were then further refined in ENVI's n-Dimensional Visualizer to identify endmembers suitable for spectral unmixing (*Table 2*).

Table 2 Lava spectral endmembers identified from the ETM+ and ALI datasets. Each endmember is characterized by the age of the lava surface relative to the image acquisition.

Lava endmembers	Vertices (*Figure 3)*	ETM+ image (31 Jan 2003)	Vertices *(Figure 3)*	ALI image (3 Jan 2012)
Young (<9 yrs.)	V6, V9	1998, 2000, 2001, 2002	V1, V4, V8	2004
Intermediate (~9-15 yrs.)	V1, V4, V8	1991-93	V6, V9	2001, 2002
Old (>15 yrs.)	V3, V7	1981-82, 1984, 1986	V3, V7	1984, 1994

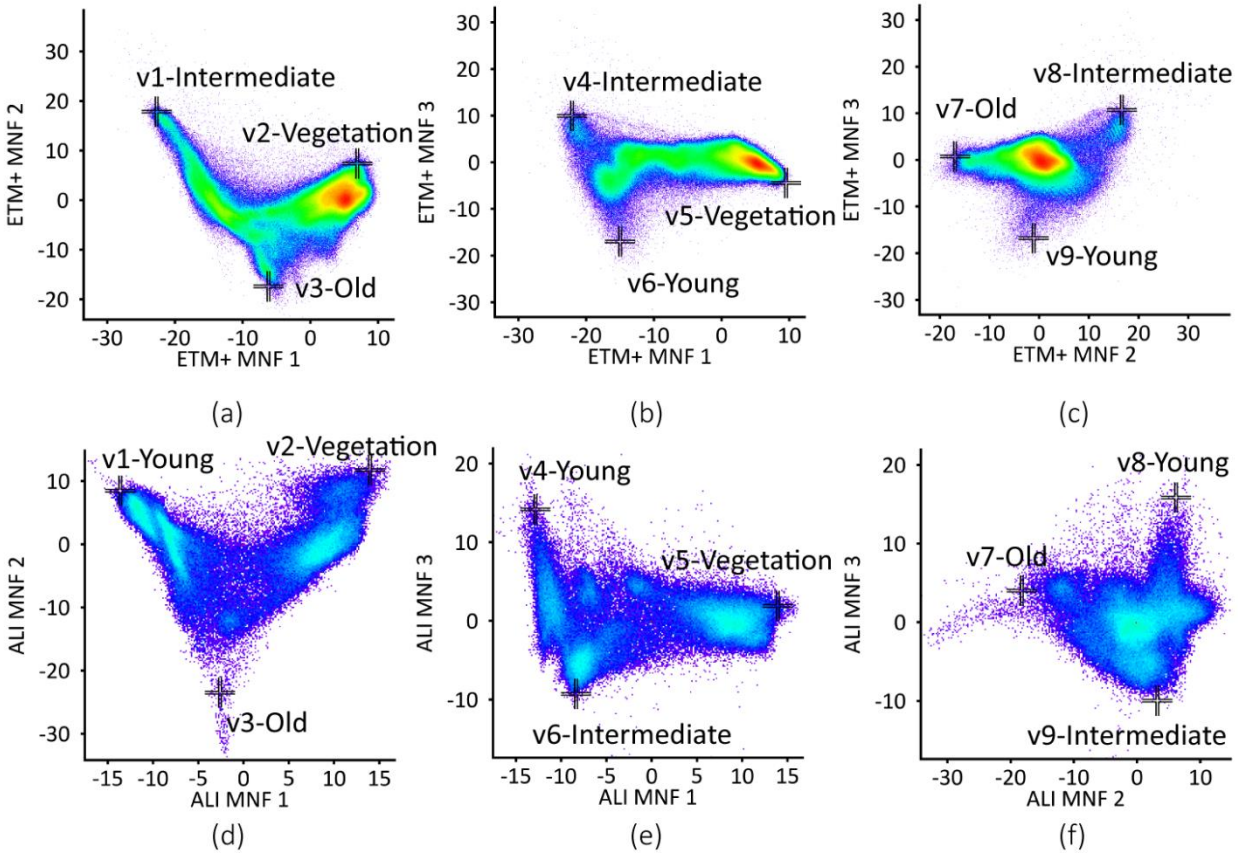

179

180 *Figure 3 Feature subspaces formed by combinations of the first three MNF components. Colors refer to*
181 *the density of pixels with red indicating highest density and purple lowest density. Panels (a) to (c) and (d)*
182 *to (f) show the ETM+ and ALI feature subspaces, respectively (see Table 2).*

183 Normalized spectra for each identified endmember are shown in *Figure 4*. In both datasets, the
184 vegetation endmember shows a local reflectance peak in band 2 (green), absorption in band 3
185 (red) and high reflectance in the NIR bands 4/4p, which is typical of vegetation spectra. For all
186 lava endmembers, the reflectance in the visible part of the spectrum (VIS, bands 1-3) is higher
187 than for the vegetation endmember. Lava spectra are characterized by an increase in
188 reflectance from the VIS to the NIR (bands 4/4p/5p) and a decrease towards the SWIR band(s)
189 5/7. It should be noted that in the ETM+ image, the spectral curve for young lava does not seem
190 to further decrease from band 5 to band 7. The old-aged lava endmember has a lower

reflectance in the VIS and a much higher reflectance in bands 5p/5 than the other two lava endmembers. The ETM+ intermediate-aged lava endmember has the highest reflectance in the VIS but the lowest in bands 5 and 7. Both the ETM+ intermediate- and young-aged lava endmembers show decreasing spectra from bands 4 to 5. The ALI intermediate- and young-aged lava endmembers show a similar shape as the ALI old-aged lava endmember, their curves rising in bands 4, 4p and 5p and then decreasing in bands 5 and 7. The old-aged lava though is clearly distinguishable from the intermediate and young-aged lava due to the higher reflectance in bands 5p and 5.

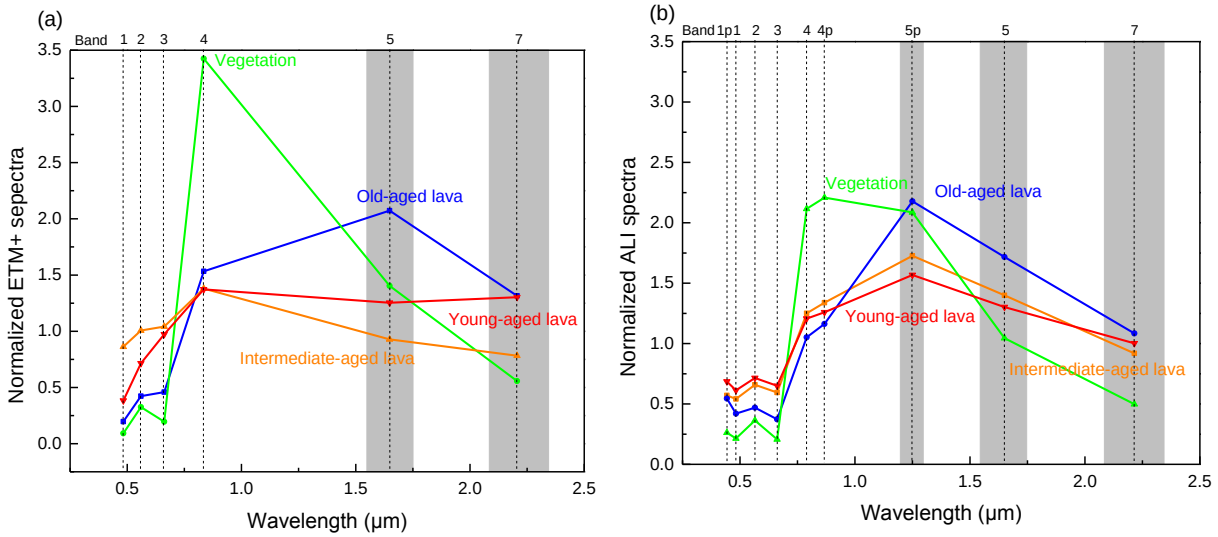

Figure 4 Normalized spectra of the four endmembers identified from the ETM+ (a) and ALI (b) datasets. Spectral bands of both images are indicated on the upper horizontal axis of each graph. The spectral ranges of bands 5p, 5 and 7 are shown by shading.

4.2 Validation of unmixing results

Once the four endmembers were identified, a fully constrained LSMA model using normalized reflectance data was applied to map endmember fractions (*Figures 5* and *6*). The average RMS of the spectral unmixing results was 0.038 for the ETM+ and 0.022 for the ALI, the latter

performing slightly better than the former in terms of model fitness (*Figure 7*). The characterization of the fresh ETM+ 2001 and 2002 flows and the area around the ALI mask with higher errors show that these areas are not well modeled by LSMA. The Pleiades image used for validation of the ALI unmixing, was classified into vegetation/lava using the Maximum Likelihood classifier with a resulting Kappa index of 0.87. Validation based on 100 randomly generated sample units was performed within the area indicated by the red rectangle in *Figure 1*. Comparison of the ALI-modeled vegetation fraction with the Pleiades-derived vegetation fraction shows that the former is lower than the latter (*Figure 8*), but the correlation between both is very high (0.963). The ME and RMSE are -0.113 and 0.210 respectively.

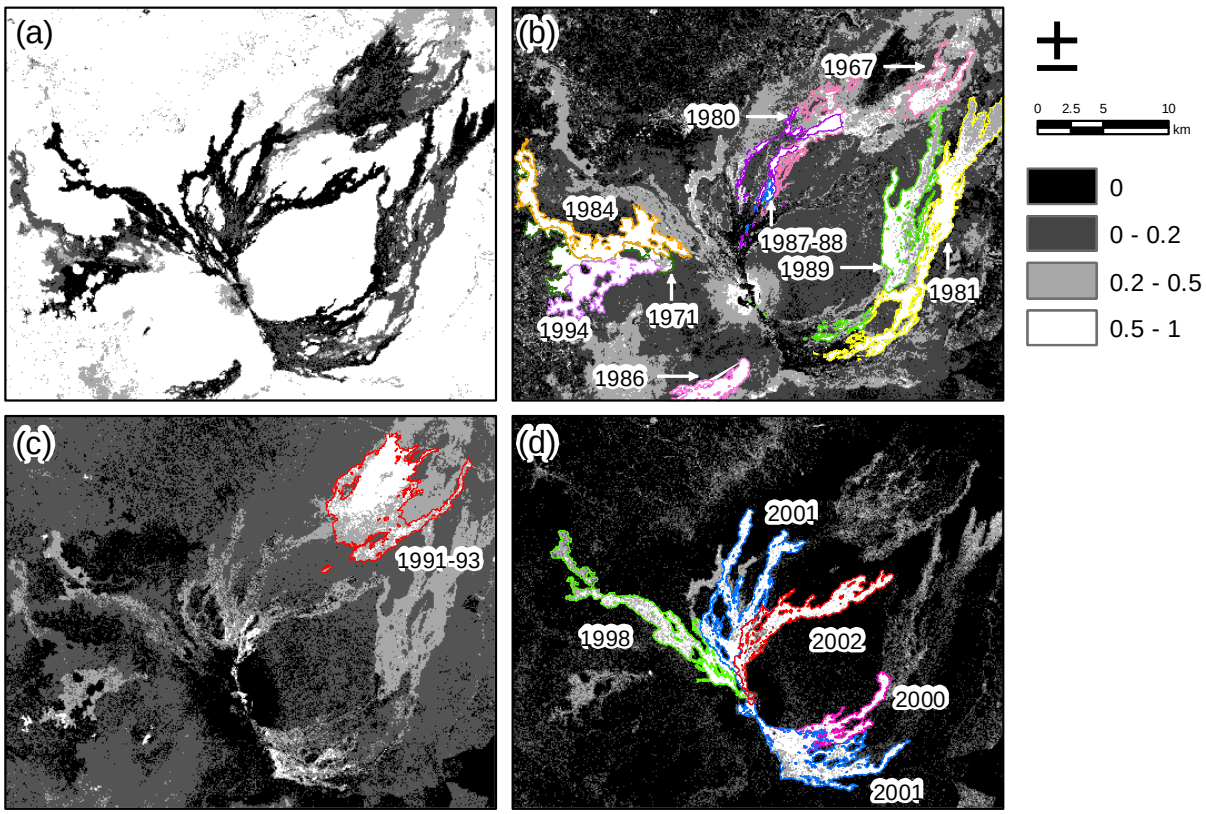

Figure 5 Fraction images derived from the ETM+ normalized reflectance data: (a) vegetation; (b) old-

aged lava; (c) intermediate-aged lava; and (d) young-aged lava. The vegetation fraction image agrees with the known vegetation distribution. The lava fraction images highlight different aged flows.

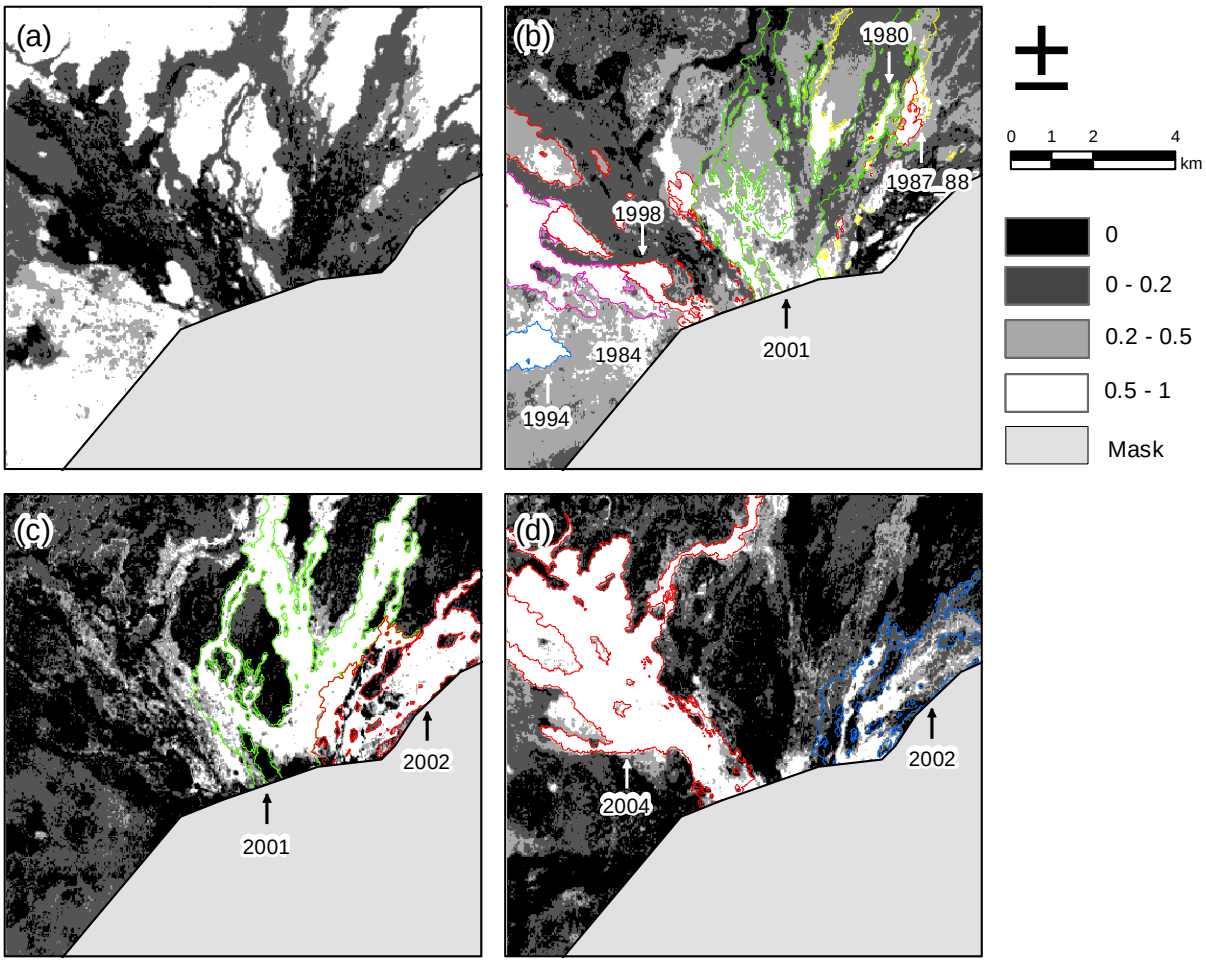

Figure 6 Fraction images derived from the ALI normalized reflectance data: (a) vegetation; (b) old-aged lava; (c) intermediate-aged lava; and (d) young-aged lava. The vegetation fraction image agrees with the known vegetation distribution. The lava fraction images highlight different aged flows.

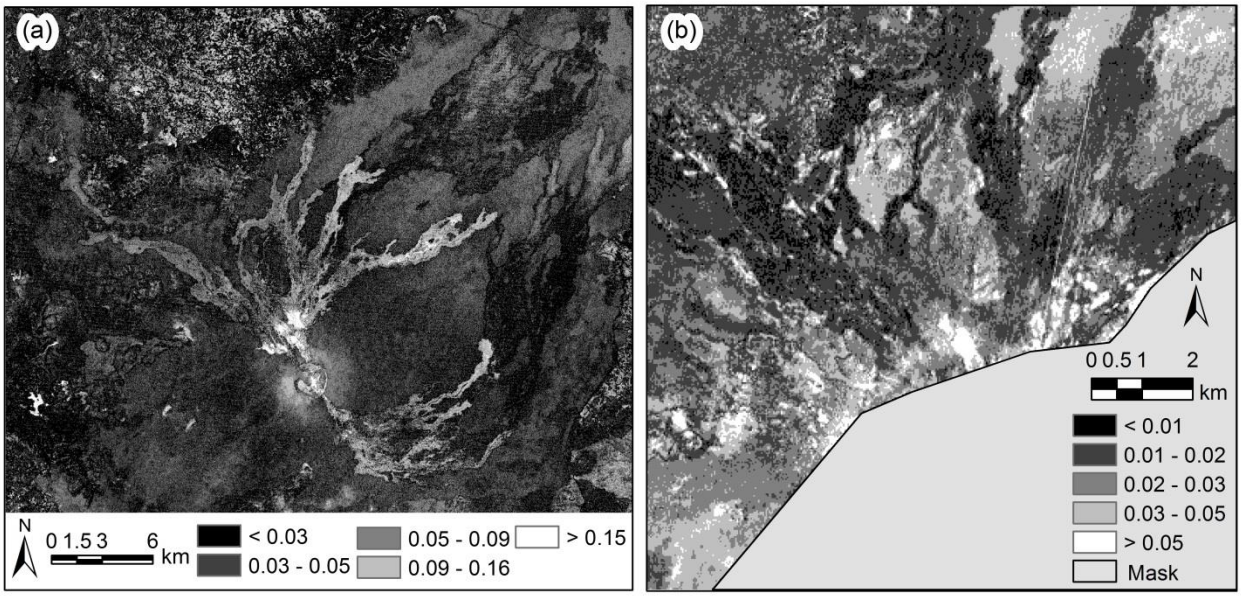

224

225 *Figure 7 LSMA RMS maps derived from the ETM+ (a) and ALI (b) images. The ALI RMS map reveals relatively high*

226 *errors in known vegetation area.*

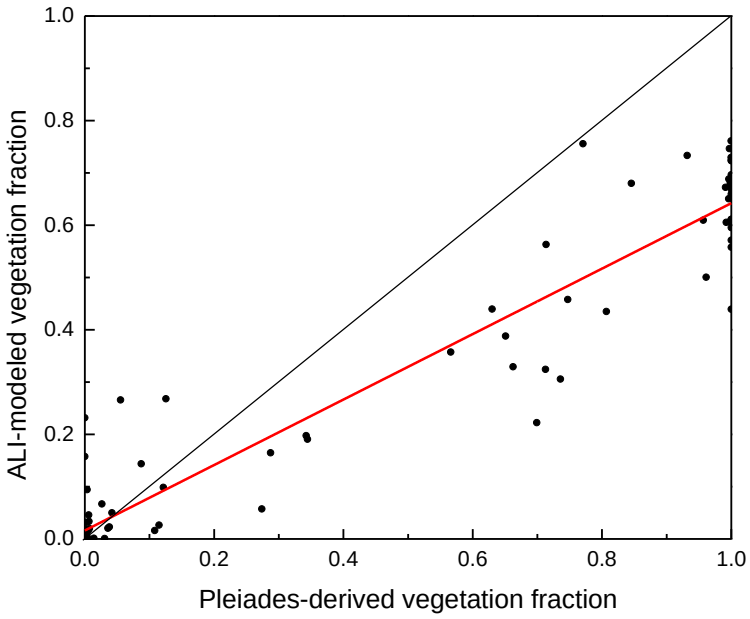

227

228 *Figure 8 Scatterplot of the Pleiades-derived vegetation fraction against the ALI-modeled vegetation fraction. It is*

229 *shown that the modeled vegetation fraction is generally lower than the reference fraction.*

4.3 Endmember fraction of lava flows

The endmember fraction images produced visually highlight different surface types. The vegetation fraction image derived from ETM+ data (Figure 5) shows vegetation fractions of known forested areas of >0.5 whereas most of fresh lava surfaces have fractions <0.2. Fraction images for the different lava endmembers clearly show contrasted lava flows, the old-aged lava fraction image showing high fraction values for the flows erupted from 1967 to 1994, the intermediated-aged fraction image for the 1991-93 flow alone and the young-aged fraction image for the flows generated between 1998 and 2002. The ALI vegetation fraction image (Figure 6) also shows very good visual agreement with known vegetated areas. The old-aged lava fraction image for ALI highlights the flows erupted from 1980 to 1998, and part of the 2001 flow. The 2001 and 2002 flows are prominent in the intermediate-aged lava fraction image, while the entire 2004 flow and part of the 2002 flow are highlighted in the young-aged lava fraction image.

For quantitative analysis, we also calculated the mean fraction of each endmember for each previously identified lava flow fields. The ETM+ image includes 21 flows erupted from 1938 to 2002, while 12 flows erupted from 1951 to 2004 are partially covered by the masked ALI image. All the flows in the two images have mean endmember fractions ranging from ~0 to >0.7 (*Figure 9*). In the ETM+ image, the 1938-40, 1951-52 and 1957 flows have very high vegetation fractions (>0.5). These values decrease gradually for more recent flows and drop to <0.1 for flows less than 13 years old. The old-aged lava endmember covers >50% on 8 flows between 8 and 32 years old. The fraction of old-aged lava is lower on more recent flows but also on those older than 32 years. The 1991-93 flow is the only one that has an intermediate-aged lava

fraction >0.5. Except for the 1956 flow, the young-aged lava fraction decreases from >0.5 to ~0 with age, reaching its highest value on the freshest 2000, 2001 and 2002 flows, and drops to < 10% for those older than 10 years. In case of the ALI image, as the lava age increases, the vegetation fraction also increases while the young-aged lava fraction decreases. The 1984, 1987-88 and 1994 flows have higher old-age lava fractions than older flows, yet the older flows also contain a significant fraction of this endmember. Highest intermediate-aged lava fractions are observed on the 2001 and 2002 flows (9-11 years after emplacement), immediately followed by the 1996 flow.

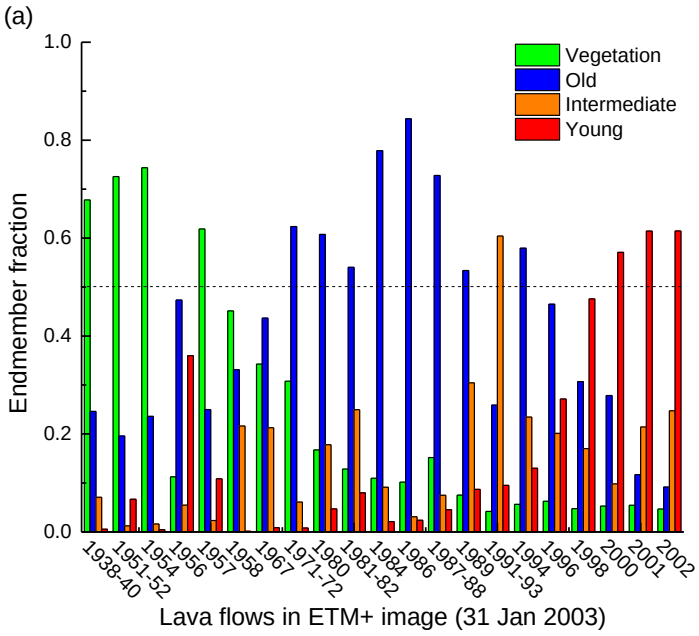

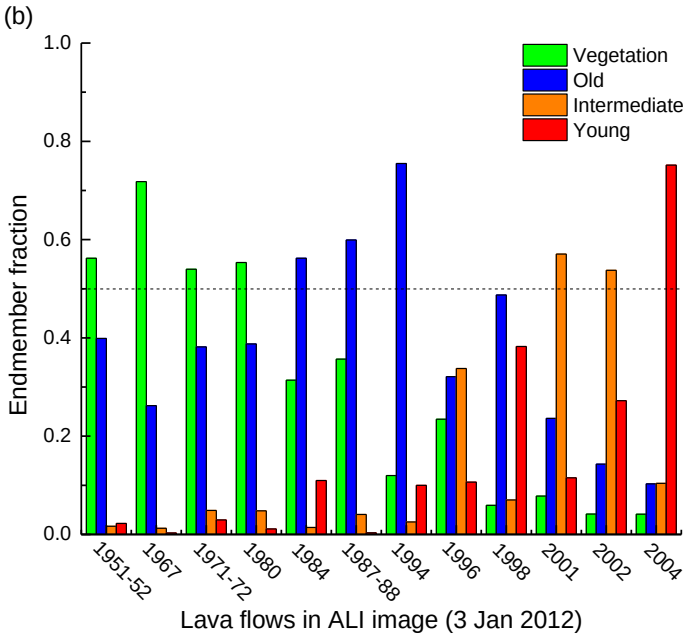

Figure 9 Mean endmember fractions for the lava flows covered (partially) by the ETM+ (a) and ALI (b) images. The fractions of each endmember change as lava ages.

Particular attention was given to the mean vegetation fraction observed for each flow. *Figure 10* presents the relationship between the mean vegetation fraction of flows and their age. The age of each flow is the interval, in decimal years, between the ending date of the lava emplacement and the acquisition date of the satellite image. The two scatter plots show that early erupted flows have a high vegetation fraction and vice versa but there are noticeable outliers. In the ETM+ scatter plot, the 1958 and 1987-88 flows are slightly offset from the main trend but the 1938-40 and 1956 flows are far from the observed trend. The only outlier in the ALI scatter plot is the 1951-52 flow. The relationship between the age of ETM+ flows and their vegetation fraction was modelled by a second order polynomial function excluding the 1938-40 and 1956 flows:

$$V = 0.0003A^2 - 0.0026A + 0.0579 \ (R^2 = 0.9746).$$

For the ALI flows, the relationship between lava age and vegetation fraction, excluding the 1951-52 flow, is linear:

$$V = 0.01802A - 0.11937 \ (R^2 = 0.9242).$$

In the two equations, V and A are the mean vegetation fraction and age of each flow.

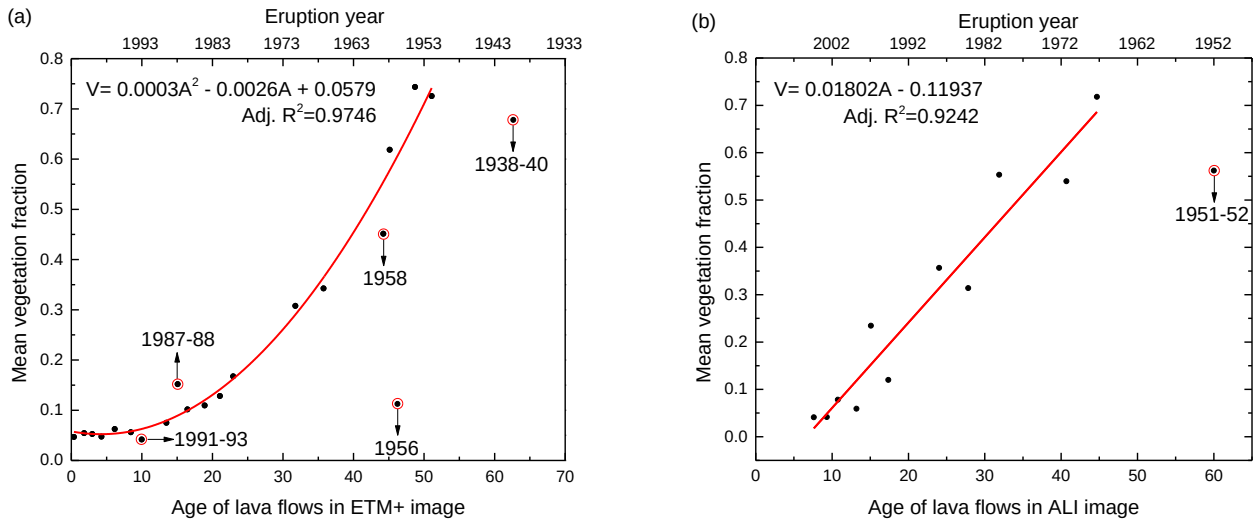

Figure 10 Scatter plots of the age of lava flows in the ETM+ (a) and ALI (b) images against their vegetation fraction.

5. Discussion

5.1 Physical meaning of endmembers

The results of this study show that LSMA clearly discriminate endmembers on the active tropical volcanic terrains analysed: irrespective of the distribution of pixels in feature space, endmember candidates lie at the vertices of the distribution, as these pixels are potentially homogenous and least correlated (Van der Meer and Jia, 2012). The feature subspaces of the

first two MNF components clearly show three vertices, suggesting that there are at least three endmembers, rather than two, i.e. vegetation and lava.

Next to a vegetation endmember, three lava endmembers are discernible in both the ETM+ and ALI feature spaces, which seem can be related to lava surfaces of different age. The clear increase in reflectance from band 3 to bands 4 (ETM+) and 4/4p (ALI), which is observed for the old-aged lava endmember, resembles the red-edge effect of vegetation (Seager et al., 2005). The increase from bands 4/4p to 5 (ETM+) and 5p (ALI) is however opposite to vegetation spectra. We suggest that this increase is due to the presence of lichens (*Figure 2(b)*) whose spectra show a gradual increase in reflectance from 0.4 to 1 µm (Rees et al., 2004).

Lava endmembers show a sharper decrease from bands 5p/5 to 7 with age, which is consistent with the fact that chemical composition change due to weathering affects the SWIR reflectance properties of lava (Ehara Suryantini et al., 2005). In contrast with the other lava endmembers, the ETM+ young-aged lava endmember shows no decrease from band 5 to 7, which can be explained by its young age. This lava endmember corresponds to very fresh flows erupted from 2000 to 2002 whereas the ALI young-aged lava endmember is characterized by flows erupted over the previous 8-10 years. Our results also demonstrate that differences in spectral properties of lavas can be used to map lava flows of different age (Abrams et al., 1996).

5.2 Accuracy of spectral unmixing

The ALI-modeled vegetation fraction is generally consistent with, but lower than the Pleiades-derived vegetation fraction. This underestimation may be due to the specification of the vegetation endmember in the LSMA model. The ALI RMS image (*Figure 7(b)*) shows that

vegetated surfaces are affected by higher unmixing errors than lava surfaces, which implies that vegetation is not well modeled in this image. Vegetation growing on volcanoes covers a wide range, including green ferns, tall trees, scattered bushes and dense grass, and only one vegetation endmember may not perfectly characterize the spectra of all the plants present on the image.

Traditional classification cannot characterize the spatial pattern and vegetation colonization range of lava surfaces. Vegetation indices such as NDVI (normalized difference vegetation index) are able to characterize the evolution of the vegetation fraction but do not capture other spectral changes associated with lava aging. Our case study of Nyamuragira's volcanic field demonstrates the potential of LSMA for identifying different lava endmembers enabling discrimination of contrasted lava surfaces. Endmember fraction distributions spatially and spectrally correspond to lava surfaces of different age. A clear interpretation of the three contrasted lava endmembers is challenging but we suggest that lichen growth and chemical weathering on lava surfaces contribute to the spectral differences between them. Improving the interpretation of the endmembers and optimizing their selection using field spectral data, which was not possible in this study due to DRC's political situation, could be a logical step to improve the obtained results. Another option might be to reduce endmember class variability by subdividing vegetation into subclasses like forest, bushes and grassland, and optimizing endmember selection for specific lava flows using multiple endmember spectral mixture analysis (Demarchi et al., 2012).

5.3 Endmember distribution of lava flows

Results show significant changes in endmember fractions over the 9 years between the two analyzed scenes: an increase in the vegetation fraction (e.g. on the 1967 and 1980 flows), a decrease in the young-aged lava fraction (e.g. by 30~50% on the 2001 and 2002 flows) and in the intermediate-aged lava fraction. These changes emphasize that endmembers are indeed related to lava surface age rather than to other surface characteristics.

Analysis of the mean vegetation fraction for each lava flow from both images reveals that, as expected, earlier erupted flows tend to have higher vegetation coverage than recently erupted ones. This finding agrees with the study of Head et al. (2013) reporting a clear increase in reflectance for the ETM+ band 4 as lava ages, and the study of Abrams et al., (1991) finding that older prehistoric flows have higher vegetation cover. The abnormal values of vegetation coverage for the ETM+ 1938-40, 1956, 1958 and 1987-88 (*Figure 10*) flows can be explained by site-specific conditions. The 1938-40 flow field has been deforested by communities progressively encroaching on the area, leading to vegetation coverage clearly lower than, for example, the 1951-52 and 1954 flows. The 1956 flow is the only one situated in Nyamuragira's caldera (above 3000 m a.s.l.), and consequently re-vegetation is much more limited. The lower vegetation fraction of the 1958 flow field is very likely the result of being partially covered by the 1991-93 flows as well as being affected by the large amount of gas and tephra emitted by this long-lasting eruption. As for the 1987-88 flows, vegetation growth might have benefited from the thin tephra layer produced by the 2001 eruption offering substrate for the initial growth of plants (Deligne et al., 2013). The ALI 1951-52 flow's low vegetation fraction probably results from tephra fallout generated by the nearby 2001, 2002 and 2004 eruptions. Repeated

exposure to tephra fall and gas from these eruptions might have degraded the vegetation, resulting in a decrease from 0.73 in 2003 to 0.56 in 2012.

The different relationship between vegetation fraction and lava age between the ALI and ETM+ data (linear and second-order polynomial) is probably due to the fact that only 2 flows less than 10 years old are present in the ALI scene compared to 7 in the ETM+ scene. It is suggested that at Nyamuragira, vegetation starts colonizing lava surfaces 10-15 years after their emplacement and occupy >50% of the lava surfaces after approximately 40 years. This finding confirms that vegetation recolonization in tropical environments occurs within a few decades after the eruption (De Rose et al., 2011). Our results obtained with the ETM+ image further suggest that vegetation recovery in these environments is slow during the first 10 years after eruptions but accelerates afterwards. The transition from bare lava to fully recovered vegetation, which is characterized by different stages of colonization by lichens and chemical alteration, can be associated to lava's spectral characteristics. This opens the possibility of using LSMA for estimating the relative age of undated volcanic surfaces and consequently supporting the evaluation of the frequency and recurrence period of effusive activity in active volcanic areas.

6. Conclusions

This study focused on the use of LSMA for characterizing Nyamuragira's lava flow fields. From our results, we conclude that:

- Linear spectral mixture analysis is capable of characterizing Nyamuragira's volcanic field and discriminating different lava surfaces.

371 •Three lava endmembers can be identified as lava of old, intermediate and young age based
372 on its spectral and spatial characteristics. It is hypothesized that the three spectrally distinct
373 lava endmembers correspond to different stages in lichen growth and chemical weathering.

374 •Vegetation fraction is highly correlated with lava age. In our study, LSMA has enabled the
375 quantification of vegetation cover with time, and hence a timeline for vegetation recovery. At
376 Nyamuragira, vegetation starts to significantly colonize lava about 15 years after eruption, and
377 occupies more than 50% of the lava surface after about 40 years.

378 This study contributes to a better understanding of the spectral evolution of lava flows with
379 time and the influence of vegetation colonization on these spectral characteristics, and also
380 demonstrates the potential of LSMA for mapping lava flows of different age based on changes
381 in spectral behaviour. The approach presented in this study could be transferred to other
382 volcanic regions characterized by lava flows of contrasted compositions or different volcanic
383 deposits.

384 ## Acknowledgements

385 L. Li wishes to acknowledge the China Scholarship Council for supporting his research at the
386 Vrije Universiteit Brussel. Thanks go to Benoît Smets for providing GIS data of Nyamuragira
387 volcano, and Prof Freek Van der Meer for his help related to the application of LSMA. The
388 Pleiades data were provided by Astrium GEO-Information Services in the framework of the
389 PLEIADES Users Group (PUG-58). This study contributes to the project GeoRisCA (SD/RI/02A)
390 funded by the Belgian Science Policy.

References

Abrams, M., Abbott, E., Kahle, A., 1991. Combined use of visible, reflected infrared, and thermal infrared images for mapping Hawaiian lava flows. J. Geophys. Res. 96, 475–484.

Abrams, M., Bianchi, R., Pieri, D., 1996. Revised Mapping of Lava Flows on Mount Etna, Sicily. Photogrammetic Eng. Remote Sens. 62, 1353–1359.

ASTRIUM, 2012. Pleiades imagery user guide. Toulouse.

Ayris, P.M., Delmelle, P., 2012. The immediate environmental effects of tephra emission. Bull. Volcanol. 74, 1905–1936.

Colclough, S., 2006. Investigations of Nyamuragira and Nyiragongo volcanoes (Democratic Republic of the Congo) using InSAR, in: Fringe Workshop. pp. 1–6.

De Rose, R.C., Oguchi, T., Morishima, W., Collado, M., 2011. Land cover change on Mt. Pinatubo, the Philippines, monitored using ASTER VNIR. Int. J. Remote Sens. 32, 9279–9305.

Del Moral, R., Grishin, S.Y., 1999. Volcanic disturbances and ecosystem recovery, in: Walker, L.R. (Ed.), Ecosystems of Disturbed Ground. Elsevier Science, pp. 137–155.

Deligne, N.I., Cashman, K. V., Roering, J.J., 2013. After the lava flow: The importance of external soil sources for plant colonization of recent lava flows in the central Oregon Cascades, USA. Geomorphology 202, 15–32.

Demarchi, L., Canters, F., Chan, J.C.-W., Van de Voorde, T., 2012. Multiple Endmember Unmixing of CHRIS/Proba Imagery for Mapping Impervious Surfaces in Urban and Suburban Environments. IEEE Trans. Geosci. Remote Sens. 50, 3409–3424. doi:10.1109/TGRS.2011.2181853

Deng, C., Wu, C., 2013. Estimating very high resolution urban surface temperature using a spectral unmixing and thermal mixing approach. Int. J. Appl. Earth Obs. Geoinf. 23, 155–164.

Ehara Suryantini, S., Van Ruitenbeek, F.J.A., Van der Meer, F.D., 2005. The effect of weathering on reflectance spectra of hydrothermal white micas and chlorites: Implications for alteration mapping, in: Jingwen, M., Bierlein, F.P. (Eds.), Proceedings of the Eighth Biennial SGA Meeting. Springer, Beijing, pp. 703–706.

Ernst, G.G.J., Kervyn, M., Teeuw, R.M., 2008. Advances in the remote sensing of volcanic activity and hazards, with special consideration to applications in developing countries. Int. J. Remote Sens. 29, 6687–6723.

Francis, P., Rothery, D., 2000. Remote Sensing of Active Volcanoes. Annu. Rev. Earth Planet. Sci. doi:10.1146/annurev.earth.28.1.81

Head, E.M., Maclean, A.L., Carn, S.A., 2013. Mapping lava flows from Nyamuragira volcano (1967–2011) with satellite data and automated classification methods. Geomatics, Nat. Hazards Risk 4, 119–144.

425 Hearn, D.R., Digenis, C.J., Lencioni, D.E., Mendenhall, J.A., Evans, J.B., Welsh, R.D., 2001. EO-1
426 Advanced Land Imager overview and spatial performance, in: IGARSS 2001. Scanning the Present
427 and Resolving the Future. Proceedings. IEEE 2001 International Geoscience and Remote Sensing
428 Symposium (Cat. No.01CH37217). IEEE, pp. 897–900.

429 Heinz, D.C., Chang, C., 2001. Mixture analysis method for material quantification in hyperspectral
430 imagery. IEEE Geosci. Remote Sens. 39, 529–545.

431 Lawrence, R., Ripple, W., 2000. Fifteen years of revegetation of Mount St. Helens: a landscape-scale
432 analysis. Ecology 81, 2742–2752.

433 Ramsey, M.S., Fink, J.H., 1999. Estimating silicic lava vesicularity with thermal remote sensing: a new
434 technique for volcanic mapping and monitoring. Bull. Volcanol. 61, 32–39.

435 Rees, W.G., Tutubalina, O.V., Golubeva, E.I., 2004. Reflectance spectra of subarctic lichens between 400
436 and 2400 nm. Remote Sens. Environ. 90, 281–292.

437 Seager, S., Turner, E., Schafer, J., Ford, E., 2005. Vegetation's red edge: a possible spectroscopic
438 biosignature of extraterrestrial plants. Astrobiology 4, 1–25.

439 Smets, B., D'Oreye, N., Kervyn, F., Kervyn, M., Albino, F., Arellano, S.R., Bagalwa, M., Balagizi, C.,
440 Carn, S.A., Darrah, T.H., Fernández, J., Galle, B., González, P.J., Head, E., Karume, K., Kavotha,
441 D., Lukaya, F., Mashagiro, N., Mavonga, G., Norman, P., Osodundu, E., Pallero, J.L.G., Prieto, J.F.,
442 Samsonov, S., Syauswa, M., Tedesco, D., Tiampo, K., Wauthier, C., Yalire, M.M., 2014. Detailed
443 multidisciplinary monitoring reveals pre- and co-eruptive signals at Nyamulagira volcano (North
444 Kivu, Democratic Republic of Congo). Bull. Volcanol. 76, 1–35.

445 Smets, B., Wauthier, C., D'Oreye, N., 2010. A new map of the lava flow field of Nyamulagira (D.R.
446 Congo) from satellite imagery. J. African Earth Sci. 58, 778–786.

447 Sohn, Y., McCoy, R., 1997. Mapping desert shrub rangeland using spectral unmixing and modeling
448 spectral mixtures with TM data. Photogramm. Eng. Remote Sensing 63, 707–716.

449 Somers, B., Asner, G.P., Tits, L., Coppin, P., 2011. Endmember variability in Spectral Mixture Analysis:
450 A review. Remote Sens. Environ. 115, 1603–1616.

451 Sonnentag, O., Chen, J.M., Roberts, D. a., Talbot, J., Halligan, K.Q., Govind, A., 2007. Mapping tree and
452 shrub leaf area indices in an ombrotrophic peatland through multiple endmember spectral unmixing.
453 Remote Sens. Environ. 109, 342–360.

454 Van de Voorde, T., De Roeck, T., Canters, F., 2009. A comparison of two spectral mixture modelling
455 approaches for impervious surface mapping in urban areas. Int. J. Remote Sens. 30, 4785–4806.

456 Van der Meer, F.D., Jia, X., 2012. Collinearity and orthogonality of endmembers in linear spectral
457 unmixing. Int. J. Appl. Earth Obs. Geoinf. 18, 491–503.

458 Weng, Q., Lu, D., Schubring, J., 2004. Estimation of land surface temperature–vegetation abundance
459 relationship for urban heat island studies. Remote Sens. Environ. 89, 467–483.

Wu, C., 2004. Normalized spectral mixture analysis for monitoring urban composition using ETM+ imagery. Remote Sens. Environ. 93, 480–492.

Wu, C., Murray, A.T., 2003. Estimating impervious surface distribution by spectral mixture analysis. Remote Sens. Environ. 84, 493–505.

Zhang, J., Rivard, B., Sánchez-Azofeifa, A., 2005. Spectral unmixing of normalized reflectance data for the deconvolution of lichen and rock mixtures. Remote Sens. Environ. 95, 57–66.